International Journal of Thermophysics, Vol. 28, No. 5, October 2007 (© 2007)
DOI: 10.1007/s10765-007-0152-8

Virtual Experiment Design for the Transient Hot-Bridge Sensor[1]

R. Model,[2,3] R. Stosch,[4] and U. Hammerschmidt[4]

The development of stable, highly sensitive sensors for measuring the thermal transport properties of a wide range of materials requires a detailed evaluation of all the effects having an impact on the measurement result. The virtual experiment design (VED), which is based on the simulation of potential experiments, offers a powerful tool to design and optimize new measurement configurations such as, for example, the transient hot-bridge sensor. The main effects of the applied simplified data analysis on the measurement uncertainty, i.e., the strip configuration, the neglected insulating foil, the linearized analysis and the shortened measurement time, are analyzed. All factors are found to be tolerable with respect to the total measurement uncertainty.

KEY WORDS: finite element analysis; measurement uncertainty; thermal conductivity; transient method; virtual experiment

1. INTRODUCTION

The development of new measurement techniques increasingly demands the numerical simulation of experiments in advance or in parallel. Such virtual experiment design (VED) based on a realistic mathematical model is a powerful numerical tool for the (a) simulation, prediction, and validation of experiments; (b) optimization of measuring instruments, e.g., geometric design of sensors; (c) cause and effect analysis; (d) case studies, e.g., material dependences; and (e) estimation of the measurement uncertainty.

[1]Paper presented at the Seventeenth European Conference on Thermophysical Properties, September 5-8, 2005, Bratislava, Slovak Republic.
[2]Physikalisch-Technische Bundesanstalt, Abbestrasse 2-12, 10587 Berlin, Germany.
[3]To whom correspondence should be addressed. E-mail: regine.model@ptb.de
[4]Physikalisch-Technische Bundesanstalt, Bundesallee 100, 38116 Braunschweig, Germany.

Often physical processes such as heat conduction are described by partial differential equations that, for more complicated situations, are only solvable by numerical analysis such as, for example, the finite-element method (FEM), which is used here for the VED. A very successful example for this is the VED-aided development of the transient hot-bridge (THB) sensor with its complicated temperature profiles. The recently introduced THB method [1] offers significant improvements vis-à-vis the well-established transient hot-strip technique (THS) [2,3] for measuring the thermal conductivity. While the latter technique uses just one metal strip as the resistive heater and thermometer, a standard THB sensor uses four parallel strips, which act simultaneously. The characteristic arrangement of all these meander-shaped two-part strips overcomes most of the drawbacks of the THS technique due to partly thermal and partly electrical compensation effects.

In Section 2 the THB technique is outlined with the underlying model. The topics of the above list of the virtual experiment design are specified according to the approximations made in the THB data analysis. The validity of the model simplifications is discussed in Section 3. Three variations of the model are analyzed: the replacement of the full-strip sensor by a meander-shaped sensor, the insertion of an insulating layer between the strip and the sample, and the shorter maximum time interval available with a linear measurement signal. Conclusions are outlined in Section 4.

2. TRANSIENT HOT BRIDGE

The thermoelectric hot-bridge sensor is based on the well-established transient hot-strip technique (THS) for measuring the thermal conductivity. The THB thermoelectric sensor is realized as a printed circuit foil of nickel between two insulating polyimide layers having an overall size of $109 \times 33 \times 0.06\,\mathrm{mm}^3$. The layout consists of four identical strips arranged in parallel and connected to form an equal-ratio Wheatstone bridge. At uniform temperature, the bridge is inherently balanced, i.e., no nulling is required prior to a run. An electric current through the unequally spaced strips establishes an inhomogeneous temperature profile that results in an unbalanced condition of the bridge. From now on, the sensor produces an offset-free output signal of high sensitivity as a measure of the thermal conductivity of the surrounding specimen. The signal is virtually free of thermal emfs because no external bridge resistors are needed. Each single strip is meander-shaped—in order to give it a higher resistivity—and, additionally, segmented into a long and a short part to compensate for the end effect, as shown in Fig. 1.

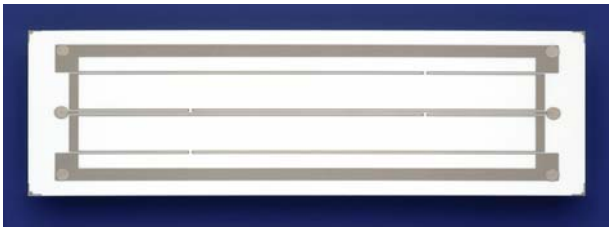

Fig. 1. Top view of the transient hot-bridge sensor layout. Each of the four tandem-strips is 100 mm in length and 2 mm in width.

The underlying three-dimensional heat conduction model can be limited to two spatial dimensions because for strips of sufficient length ($L \geqslant 100$ mm), heat losses at both ends are negligible. Hence, the heat conduction equation may be defined in a cross-sectional area perpendicular to the strips. Due to the symmetrical setup, the numerical integration domain can be reduced to a quarter of the cross-sectional area as shown in Fig. 2. It leads to the differential equation,

$$\frac{\partial T(x, y, t)}{\partial t} = \text{div}\ (a(x, y)\,\textbf{grad}\, T(x, y, t)) + \frac{a(x, y)}{\lambda(x, y)} q(x, y) \tag{1a}$$

with the initial condition,

$$T(x, y, 0) = T_0, \quad (x, y) \in \Omega = [0, l] \times [0, d] \tag{1b}$$

and boundary conditions of the third kind at the sample surface,

$$-\lambda \frac{\partial T}{\partial \boldsymbol{n}} = h(T(x, y, t) - T_0), \quad x = l, y \in [0, d] \text{ or } x \in [0, l], y = d \tag{1c}$$

and vanishing heat flux at the axes of symmetry ,

$$-\lambda \frac{\partial T}{\partial \boldsymbol{n}} = 0, \quad x = 0, y \in [0, d] \text{ or } x \in [0, l], y = 0. \tag{1d}$$

The real model distinguishes three types of material: the sample (λ_S, a_S), the insulating layer (λ_L, a_L), and the metal of the strip (λ_m, a_m), whereby the thermal conductivity λ and the thermal diffusivity a in Eq. (1) are updated according to the spatial position. The heat source q is applied to the strips equally distributed.

The data analysis for THB is based on the following assumptions: (a) the two pairs of outer strips (see Fig. 2) are modeled as two single strips of width d and the four inner strips are modeled as one single strip of width $2d$; (b) the insulating foil is ignored; and (c) the signals

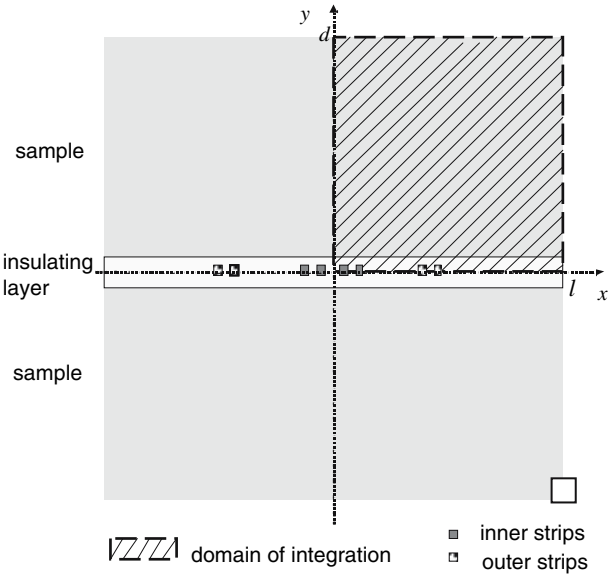

Fig. 2. Schematic cross section through the sample perpendicular to the strip. The size of the metal strips and the insulating foil thickness are exaggerated.

are calculated according to the linearized Gustafsson's approximation. As a result, the thermal conductivity of the sample is determined by means of the slope m_{THB} of the linear part of the measurement signal (difference between the voltage drop of the inner and outer sensor parts);

$$\lambda = \frac{\alpha R_0^2 I_{\mathrm{B}}^3}{2\pi L m_{\mathrm{THB}}} \tag{2}$$

where I_{B} is the constant current input, R_0 is the effective resistivity, α is the temperature coefficient of the electrical resistance, and L is the length of the meandered strips (see Ref. [1]).

In Sections 3.1 and 3.2, assumptions (a) and (b) are checked for validity. The applicability of assumption (c) was verified, e.g., in Refs. [3] and [4]. However, because of the superposition of temperature distributions caused by the inner and outer strip sources, the linear part of the measurement signal will be treated briefly in Section 3.3.

3. VIRTUAL EXPERIMENT

So far, an analytical solution to the model equation, Eq. (1), for the structure shown in Fig. 2 is not available, but for numerical procedures

such as the finite-element method (FEM), Eq. (1) is no problem. Here, we use the FEM solution for a thorough check of the simplifications made in the THB data analysis.

3.1. Meander Shape Compared to Full Strip

First, we replace the meander structure of the sensor by full strips, one in the inner position and one in each half width in the outer position. The rate of heat flow remains the same. However, the source $q[\mathrm{W{\cdot}mm^{-2}}]$ is given per unit area (in the two-dimensional case) and has to be adapted to the altered geometry. Figure 3 shows the temperature rise for both the meander-shaped sensor and the full-strip sensor on the axis $y=0, x \geqslant 0$ for the case of isothermal boundary conditions, with BK7 having been chosen as the sample material ($\lambda_S = 1\,\mathrm{mW{\cdot}m^{-1}{\cdot}K^1}$, $a_S = 0.5\,\mathrm{mm^2{\cdot}s^{-1}}$). The full profile may be obtained by reflection with respect to the y-axis. Clearly visible are the sharp local maxima of the four strips of the meandered sensor compared to full strips of adequate width. The thermal conductivity of the foil, $\lambda_L = 0.2\,\mathrm{mW{\cdot}m^{-1}{\cdot}K^{-1}}$, is much smaller than that of the metal strip, $\lambda_m = 69.1\,\mathrm{mW{\cdot}m^{-1}{\cdot}K^{-1}}$, and so are the thermal diffusivities, $a_L = 8.7\,\mathrm{mm^2{\cdot}s^{-1}}$ and $a_m = 0.2\,\mathrm{mm^2{\cdot}s^{-1}}$, respectively. Therefore, the temperature difference between the strips remains relatively small, independent of the measurement period. As expected, the temperature in the strip located closest to the sample surface is the first one to be influenced by the boundary. However, for a period of about 100 s, the temperature

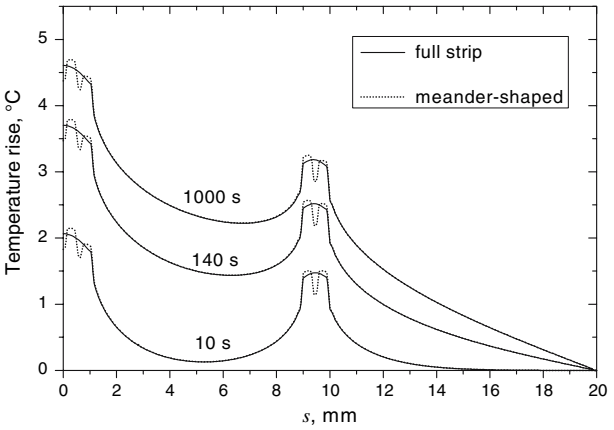

Fig. 3. Temperature rise on the horizontal axis of symmetry [(0,0),(l,0)] for meandered sensor and full-strip sensor for different periods.

distribution is identical in both outer strips and the interaction between the inner and outer strips is negligible. Over the whole measurement period, the temperature rise in the meandered strips is higher than for the case of full strips. This is due to the fact that heat conduction slows down in the gaps between the strips close to each other, which can also be seen in Fig. 4a. The difference between the signals of different boundary conditions, adiabatic and isothermal, indicates the influence the surface has on the strip temperature. In this example a strong effect is clearly seen after 100 s. However, the main question we ask ourselves is: Can we replace the mathematical model of the meander-shaped sensor by a full strip model ? The answer is positive, we can replace it. An FEM-simulated example of a more detailed investigation shown in Fig. 4b gives good agreement between both.

3.2. Measurement Uncertainty Caused by the Insulating Foil

For the case where pure metal strips are embedded into the specimen (as in the THS technique), conducting materials such as metals, wetted solids, or dissolved electrolytes are generally excluded from the analysis, as they would cause a short circuit. These restrictions can be overcome by inserting insulating layers (such as, for example, thin polymer foils) between the strip and sample. Additionally, the foils will protect the sensor from mechanical destruction and atmospheric corrosion. However, the additional foils can affect the THB signal adversely and subsequently the uncertainty in the same manner.

The effect an insulating foil has on the measurement uncertainty was examined carefully for a single strip, thus avoiding the interaction of different error sources [5]. The setup corresponds to the THS method, where the strip acts at the same time as a heat source and a resistance thermometer. Its temperature-dependent voltage drop in time is a measure of the thermal transport properties. Separating the sensor and the sample halves by inserting an additional layer changes, however, the thermal part of the setup into a two-layer system that is not represented by the underlying mathematical model. In fact, measuring the individual thermal transport properties of two-layered materials from a single THS run is a complicated task because an analytic model is not yet available. Recently, Model et al. [6, 7] have developed a procedure for layered composites based on finite element solutions of the heat conduction equation and an optimization strategy. Here, the question should be answered whether or for which materials the effect of the additional layer on the measurement result remains small even though the underlying mathematical model describes a one-layer system only.

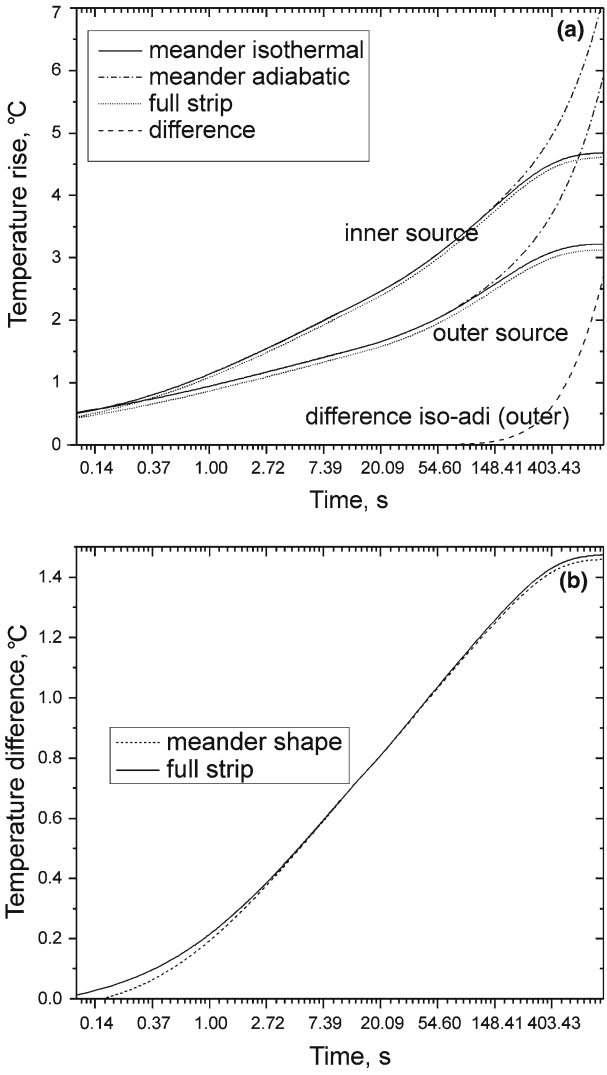

Fig. 4. (a) Temperature rise in the inner and outer sensors for both the meander-shaped and full-strip sensor structures and (b) THB signal for meander-shaped and full-strip sensors.

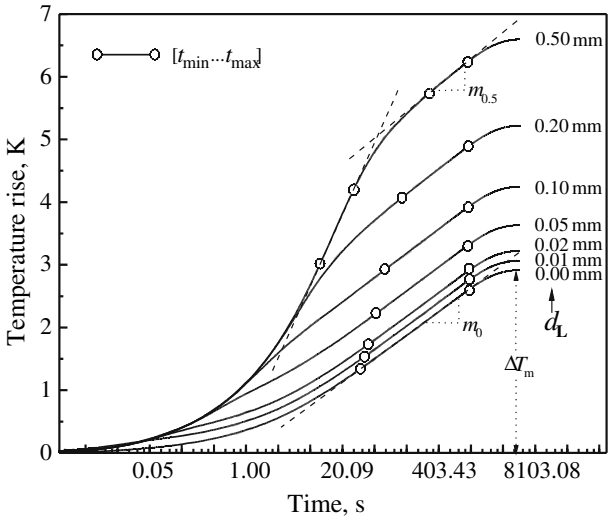

Fig. 5. FEM-simulated signal for varying layer thicknesses.

In the following, at first, some principal trends of changes in the THS signal, caused by an additional insulating layer, will be discussed in detail, and then the resulting uncertainties will be analyzed. When increasing the layer thickness d_L, three effects on the shape of the recorded temperature versus $\ln t$ curve can be observed (see Fig. 5). In practice, an electrically insulating layer with a thickness of up to 0.1 mm is more interesting. Both curves for thicker layers illustrate the continuing changes in properties.

First, with increasing layer thickness, the width of the time interval with a linear temperature versus $\ln t$ is decreasing. While the upper limit in time, t_{max}, remains fixed, the lower limit, t_{min}, is shifted towards longer periods of time. When the layer thickness exceeds a certain threshold value, the insulation itself behaves like a specimen and forms a corresponding linear segment. With the layer thickness further increasing (not shown in Fig. 5), the linear part vanishes completely.

Second, the maximum temperature excursion, ΔT_m, increases. This quantity would be measured in a quasi-steady state, i. e., under isothermal boundary conditions, and depends on the thickness and thermal properties of the materials concerned. In the present case the thermal diffusivity of the layer a_L is smaller than that of the sample a_S. In the opposite case, the maximum temperature would decrease.

Finally, the slope m of the linear part of the curve changes. In Fig. 5, for instance, m gradually increases ($m_{0.5} > m_0$), leading to an

underestimation of the thermal conductivity. Here, the thermal diffusivity of the foil a_L was chosen smaller than that of the sample a_S. In the opposite case an overestimation would be noticeable. The latter finding clearly illustrates the limits of the current mathematical model. The signal resulting from a two-layer setup does not simply equal the sum of two successive signals that would result from a single-layer setup.

In the next step, measurement signals were simulated considering the insulating foil. To re-identify the thermal conductivity from the temperature versus ln t plot, the slope m of the linear interval yields λ_R corresponding to the usual THS equation,

$$\lambda_R = \frac{\alpha U_0^2 I}{4\pi L m} \tag{3}$$

is determined and evaluated according to Eq. (3). The relative error (in %) in the thermal conductivity $u_L(\lambda)$ caused by the presence of the insulating layer is then defined by

$$u_L(\lambda) = \frac{\lambda_R - \lambda}{\lambda} 100 = \frac{\Delta\lambda}{\lambda} \tag{4}$$

where λ and λ_R are the input value and the re-identified value of the thermal conductivity, respectively. The input parameters used for the simulations were chosen in such a way that they meet the requirements of practical applications. To embed the metal strip, two possible candidate materials have been selected: polytetrafluoroethylene (Teflon) and polyimide (Kapton). These two polymers are chemically inert, resist temperatures of up to 250°C, and provide sufficient mechanical flexibility. Hence, the thermal transport properties of the layer were chosen equal to a typical polymer ($\lambda_L = 0.2\,\mathrm{W{\cdot}m^{-1}{\cdot}K^{-1}}$; $a_L = 0.16\,\mathrm{mm^2{\cdot}s^{-1}}$) and kept constant throughout all simulation runs.

To investigate the dependence of $u_L(\lambda)$ on the layer thickness, two series of simulations were carried out. In each series, either the thermal conductivity ($\lambda_S = 1.0\,\mathrm{W{\cdot}m^{-1}{\cdot}K^{-1}}$) or the thermal diffusivity ($a_S = 1.0\,\mathrm{mm^2{\cdot}s^{-1}}$) of the specimen was kept constant while the other property was varied within an appropriate range, a_S = 0.2–5.0 $\mathrm{mm^2{\cdot}s^{-1}}$ and accordingly λ_S= 0.2–5.0 $\mathrm{W{\cdot}m^{-1}{\cdot}K^{-1}}$. These combinations of λ_S and a_S cover several materials, such as mortar, Pyrex, or granite. According to Fig. 6, where the thermal conductivity and the thermal diffusivity were plotted on a double logarithmic scale, nearly all solids fall within a limited area close to the bisecting line between the x and y axes. The values are taken from Ref. [8]. Considering the fact that only a few of the chosen λ_S/a_S combinations are of practical relevance (cf. Fig. 6), a thickness between 20 and 50 μm seems to be a good choice.

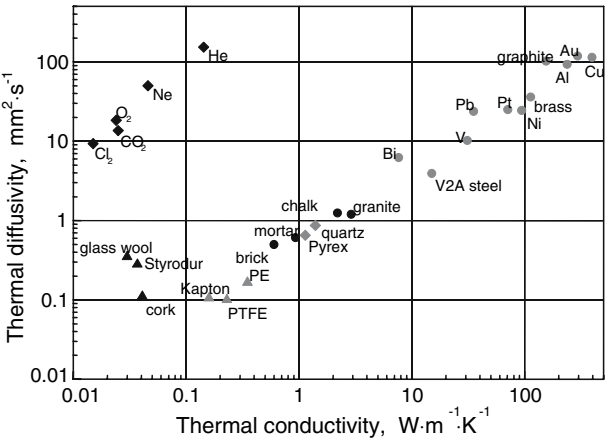

Fig. 6. Diagram of the thermal transport properties of different materials.

Thickness values of 20 and 50 μm are examined in a more extensive series of virtual experiments quantifying the additional measurement uncertainty caused by the insulating layer. The results are presented in Fig. 7, where for the two-layer thicknesses the relative error in the thermal conductivity (Eq. (6)) against the thermal conductivity of the sample, λ_S, is shown for varying thermal diffusivity a_S. For the layer, the thermal properties of a typical polymer, $\lambda_L = 0.2\,\mathrm{W{\cdot}m^{-1}{\cdot}K^{-1}}$; $a_L = 0.16\,\mathrm{mm^2{\cdot}s^{-1}}$, were chosen. Distinguishable are an overestimation of λ_S with a positive sign of $\Delta\lambda\lambda$ in the upper part and an underestimation with a negative sign of $\Delta\lambda/\lambda$ in the lower part caused by the property $a_L < a_S$, and *vice versa*, respectively. Surprisingly, in the special case of $a_L = a_S$, the additional part of uncertainty vanishes, which means the results coincide with the standard THS technique. As already shown in Figs. 4 and 5, a thicker insulating layer leads to a considerable increase in the uncertainty. For fixed a_S and increasing λ_S, the term $\Delta\lambda/\lambda$ tends towards zero or, in other words, the materials with a higher thermal conductivity yield a smaller uncertainty than the others. Using polyimide as the insulating material and considering only those pairs of values for λ_S and a_S which may occur in practice, the contribution to the uncertainty does, for layer thicknesses of 20μ m, not exceed 2%. For thinner layers, the uncertainty caused by the insulation is accordingly smaller. The presented method yields an effective tool to estimate this uncertainty caused by an additional layer of any material and thickness.

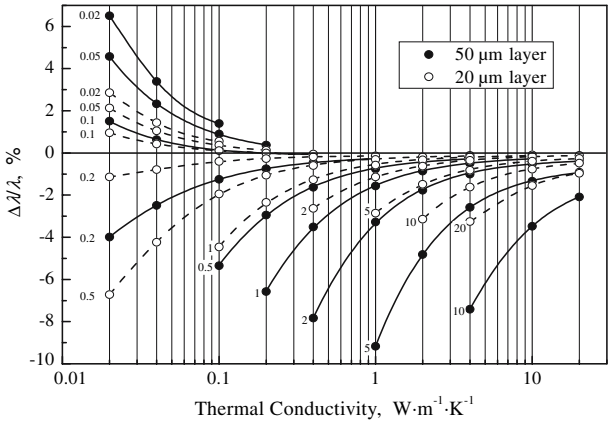

Fig. 7. Relative error in the thermal conductivity $\Delta\lambda/\lambda$ (Eq. (6)), plotted against the thermal conductivity of the sample (for different thermal diffusivities and layer thicknesses).

The numerical results coincide with experiments having been carried out with the reference material Pyrex and with Kapton foils of different thickness.

3.3. Time Interval of Measurement

For the standard THS the data analysis is practically valid only in a limited time window determined by

$$[t_{\min}, t_{\max}] = \left[\frac{D^2}{a}, \frac{0.18R^2}{a}\right] \tag{5}$$

where D denotes the strip width and R is the minimum distance between the center of the sample and its outer surface [4]. Within the interval of Eq. (5), the THS signal is a straight line when plotted against $\ln t$. The thermal conductivity λ and the thermal diffusivity a can be obtained directly from the slope and intercept, respectively. For the THB technique, the problem is more complicated because the inner and outer strips interact with each other. The movie frames in Fig. 8 show the heat conduction in the first time interval of 50 s. The question of interaction we will illustrate by an example, again with FEM simulation for BK7 samples. Figure 9 shows the time-dependent temperature rise curves both for the THB source combination and the individual heat source in the inner and outer positions, respectively. The start of interactions between the inner and outer sources is given at the branch points of the curve couples. The

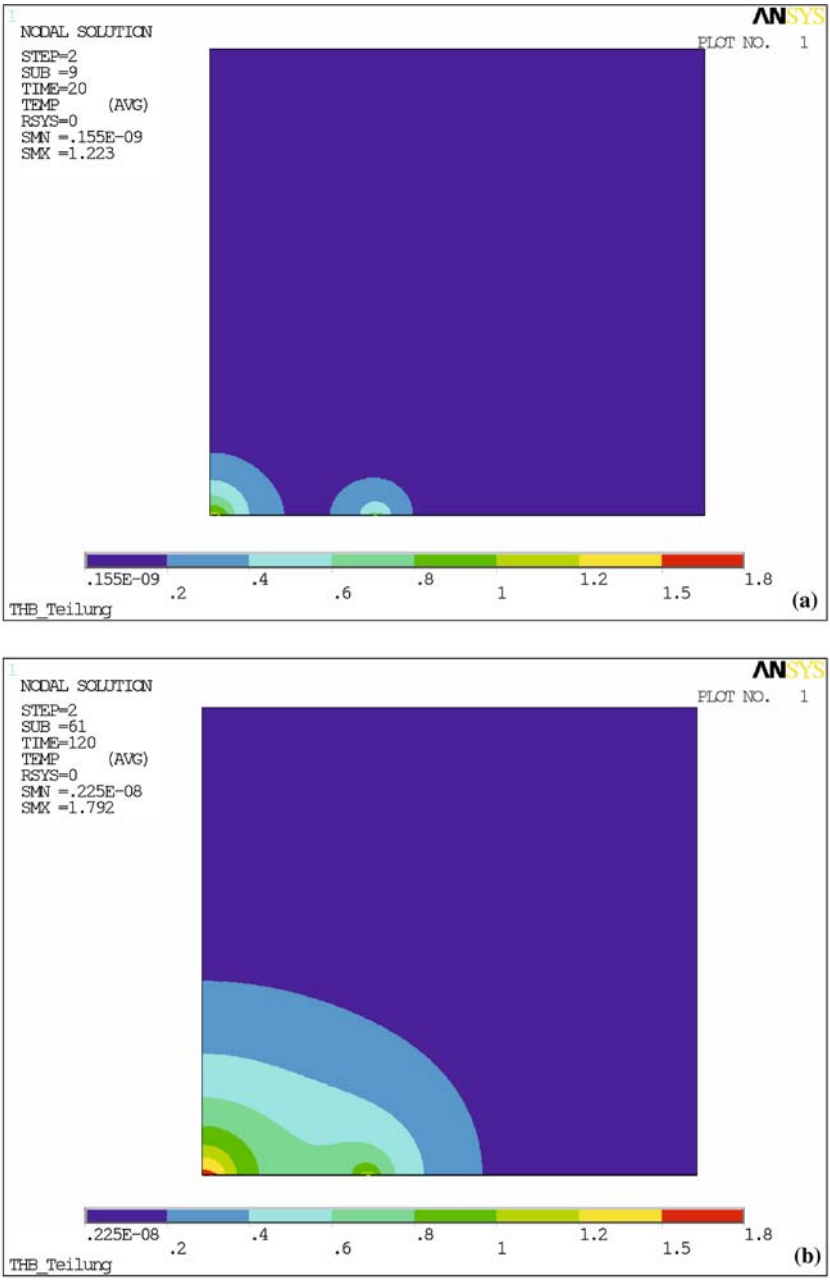

Fig. 8. Temperature distribution (a) after 20 s and (b) after 120 s.

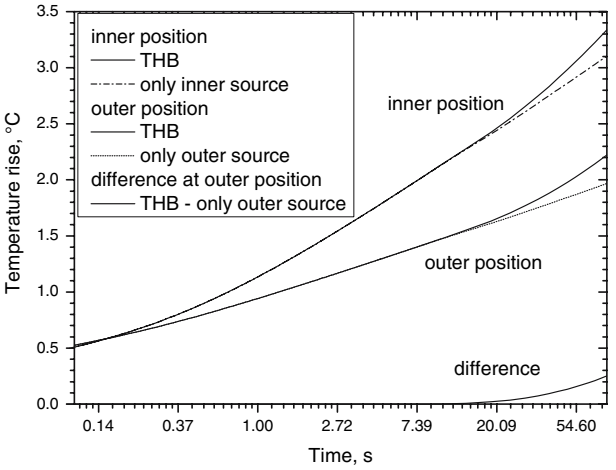

Fig. 9. Time-dependent temperature rise for the inner and outer strips for the THB technique and individual heat sources. Lower curve: difference between the temperature rise in the outer position for THB technique and individual outer source.

red curve representing the temperature difference in the outer position between the combined THB sources and the individual outer source, i.e., the lower couple, indicates at about 25 s the start of interactions which are not to be neglected. In contrast to the THS technique (see Eq. (5)), the maximum time interval with a linear measurement signal does not depend on the distance to the surface but on the distance b between the inner and outer strips. It can be expected that for the maximum measurement time,

$$t_{\max} = \frac{0.18b^2}{a} \tag{6}$$

holds, which coincides with Fig. 9. The sample size characterized by R should be greater than the distance b, because the entire THB sensor has to be covered by the sample. Therefore, the maximum time interval available with a linear measurement signal is shorter with the THB than with the THS for a given sample or sensor size. However, the maximum time interval for the THB remains sufficiently long in order to determine the thermal conductivity and thermal diffusivity.

4. CONCLUSIONS

The transient hot-bridge sensor based on the idea of the transient hot-strip technique, overcomes its major drawbacks but preserves all of

the advantages of the THS. Although the sensor structure is more complicated, the principles of the THS data analysis remain valid, as demonstrated by the virtual experiment design. Three variations of the model were analyzed: the replacement of the full-strip sensor by a meander-shaped sensor, the insertion of an insulating layer between the strip and the sample, and the shorter maximum time interval available with a linear measurement signal. As a result, the measurement uncertainty remains in the same range as for the case of the THS technique. So far, no adequate analytical solution of the related heat conduction equation is known; thus, the simplifications of the mathematical model are carefully checked by FEM simulations for both the THB and THS sensors. Previous measurements on BK7 and the reference material PMMA confirm the idea.

REFERENCES

1. U. Hammerschmidt, V. Meier, and R. Model, in *Proc. 28th Int. Thermal Cond. Conf.* (St.-Andrews-by-the-Sea, New Brunswick, Canada, 2005), pp. 278–287.
2. S. E. Gustafsson, E. Karawacki, and M. N. Khan, *J. Phys. D* **12**:1411 (1979).
3. U. Hammerschmidt, *Thermal Conductivity* **24**:123 (1999).
4. R. Model and U. Hammerschmidt, in *Advanced Computational Methods in Heat Transfer VI*, B. Suden and C.A. Brebbia, eds. (WIT Press, Ashurst, Southampton, UK, 2000), pp. 407–416.
5. R. Model, R. Stosch, and U. Hammerschmidt, in *Proc. 28th Int. Thermal Cond. Conf.* (St.-Andrews-by-the-Sea, New Brunswick, Canada, 2005), pp. 298–308.
6. R. Model and U. Hammerschmidt, in *Thermal Conductivity 26/Thermal Expansion 14*, R. B. Dinwiddie and R. Mannello, eds. (DEStech Pubs., Lancaster, Pennsylvania , 2005), pp. 346–357.
7. R. Model and U. Hammerschmidt, *High Temp.–High Press.* **34**:649 (2003).
8. Y. S. Touloukian, R. W. Powell, C. Y. Ho, and P. G. Clemens, in *Thermophysical Properties of Materials* (Plenum Press, New York, 1979).